

# A vapor-cell clock with fractional frequency reaching $10^{-16}$ level stability

Siqi Wu<sup>1,4</sup>, Zhenqi Zhang<sup>1,4</sup>, Xingyue Liu<sup>1</sup>, Chuanshuai Zhu<sup>1</sup>, Zhiyuan Wang<sup>1</sup>, Zhiyu Ma<sup>1</sup>, Hongli Liu<sup>1</sup>, Wenhao Yuan<sup>1</sup>, Xiaochi Liu<sup>2</sup>, Pengfei Wang<sup>2</sup>, Feng Zhao<sup>2</sup>, Jan Hrabina<sup>3</sup>, Jie Zhang<sup>1</sup>, Zehuang Lu<sup>1</sup> and Ke Deng<sup>1\*</sup>

<sup>1</sup> National Gravitation Laboratory (NGL), School of Physics, Huazhong University of Science and Technology, Wuhan 430074, China;

<sup>2</sup> Key Laboratory of Atomic Frequency Standards, Innovation Academy for Precision Measurement Science and Technology, Chinese Academy of Sciences, Wuhan 430071, China;

<sup>3</sup> Institute of Scientific Instruments of the Czech Academy of Sciences, Královopolská 147, 61264 Brno, Czech Republic;

<sup>4</sup> These authors contributed equally to this work.

\*ke.deng@hust.edu.cn

## ABSTRACT

Compact optical clocks with high stability are essential for next-generation frequency standard field applications, from navigation to geodesy, yet existing vapor-cell clock systems have remained confined to fractional instabilities over  $10^{-15}$ . Here, we report the breaking of this long-standing barrier by demonstrating a molecular iodine optical clock that reaches an instability of  $6.6 \times 10^{-16}$  at 1000 s and consistently operates at the  $10^{-16}$  level throughout 100–2000 s—surpassing all previous vapor-cell standards by nearly an order of magnitude. This achievement is enabled by a special design architecture that integrates a monolithic, drift-immune spectroscopic unit bonded to an ultra-low-expansion glass substrate with active temperature control of key components. The whole system only occupies 25 L. The system achieves  $5 \times 10^{-15}$  instability at 1 s and sustains  $10^{-16}$ -level performance over hours, representing the first medium-term optical stability at this level from a compact, field-ready package. Our work establishes that  $10^{-16}$  fractional frequency instability can be engineered into robust, portable systems through holistic stability-conscious design, opening a path towards high-precision time-keeping beyond the laboratory environment.

Precision time-keeping is a cornerstone of modern science and technology research. Optical clocks based on laser-cooled atoms or ions can now reach instabilities below  $10^{-18}$ , enabling unprecedented tests of fundamental physics<sup>1-5</sup>. Yet their size, fragility and complexity confine them to laboratories, creating a gap between their potential and their field deployability for critical applications such as next-generation satellite navigation<sup>6,7</sup>, autonomous time-keeping in field environments<sup>8</sup> and Very Long Baseline Interferometry (VLBI)<sup>9</sup>. Bridging this gap requires a paradigm shift towards robust, compact, and energy-efficient clock architectures that do not compromise core performance metrics.

Vapor-cell clocks, in which atoms are confined in a simple glass cell, offer a promising route towards such miniaturization and operational simplicity. Among these, the molecular iodine clock—one of the earliest platforms for optical clock demonstration<sup>10,11</sup> and a long-established length standard<sup>12-17</sup>—is undergoing a renaissance. Its low sensitivity to external fields and the mature, frequency-doubled Nd:YAG laser technology<sup>18</sup> that underpins it have driven decades of metrological refinement. Today, this system is finding renewed relevance in space-based missions<sup>19-22</sup> and field-deployable time-keeping<sup>23</sup>. Yet, despite decades of refinement, the best iodine cell clocks have plateaued at fractional frequency instabilities around the

$10^{-15}$  level at best<sup>21,23-25</sup>. This limit has been imposed by fundamental challenges including the homogeneous broadening of the transition under room-temperature operation<sup>26</sup>, collisional frequency shifts<sup>27</sup>, and technical laser noise. Consequently, the scientific community has widely regarded vapor-cell systems as secondary standards, inherently incapable of reaching the ultra-stable regime ( $10^{-16}$  and beyond) required for the most demanding future applications.

Here, we break this barrier through a holistic stability-engineering strategy. Using the R(56)32-0: $a_1$  line and modulation-transfer spectroscopy (MTS) in a specified saturation pressure (3.3 Pa) cell, we construct a clock whose core is a monolithically integrated spectroscopic module: the iodine cell, interference filters and photodetector are permanently epoxy-bonded onto a single ultra-low-expansion glass substrate, effectively suppressing beam pointing drift and achieving exceptional structural stability. This alignment-free core is then housed within a hermetically sealed, precision temperature-stabilized oven, providing a first protection against environmental fluctuations. We extend the same philosophy to active components, implementing independent, high-precision temperature control of the external electro-optic modulator (EOM) and active laser-power stabilization.

This design architecture helps to yield a fractional frequency instability in the mid- $10^{-15}$  range at 1 second. More importantly, in the critical 100-second to 2000-second window essential for applications using flywheel local oscillator and coherent signal integration, the instability remains in the  $10^{-16}$  level. These results represent the first demonstration of a vapor-cell optical standard attaining the  $10^{-16}$ -level stability in the medium-term stability regime essential for global navigation, VLBI and autonomous field operation. The current system exhibits a long-term drift on timescales beyond  $10^4$  s. This drift is attributed to residual effects of the temperature control and laser power control and presents a clear target for future refinement. Our work reestablishes molecular iodine as a primary candidate for next-generation compact optical clocks, proving that drift-immune monolithic integration coupled with targeted active-component control can deliver cold-atom-optical-clock grade stability in a robust, field-ready package.

## Results

To achieve frequency discrimination of the hyperfine transition in molecular iodine, we employed modulation transfer spectroscopy and frequency-locked the 532 nm laser output to the R(56)32-0: $a_1$  hyperfine transition line. A schematic of the setup is shown in Fig. 1(a). The system is based on a Nd:YAG solid state laser that simultaneously emits at 1064 nm and 532 nm. The 532 nm output first passes through an optical isolator, a half-wave plate (HWP), and a polarizing beam splitter (PBS), which divides it into two beams: the transmitted beam serves as the pump beam, while the reflected beam acts as the probe beam. The pump beam is frequency-shifted by 100 MHz using an acousto-optic modulator (AOM) and subsequently phase-modulated via a resonant (325 kHz) EOM. The EOM is a wedged electro-optic modulator housed within an individual temperature-stabilized enclosure for precise thermal control. The modulation depth is 1.38. The weaker probe beam is shifted by 80 MHz with a separate AOM. Both beams are coupled into polarization-maintaining fibers using fiber couplers and delivered to the iodine spectroscopy module (ISM). After integrating part of the optical path onto the substrate, the whole system only occupies 25 L.

The ISM is shown in the white substrate region in Fig. 1(a), and its internal physical photograph is displayed in Fig. 1(b). The ISM is housed on a ULE glass block substrate with dimensions  $33 \times 11 \times 3$  cm<sup>3</sup>. The mirrors, wave plates and PBS/BS are made of fused silica, and the window surfaces have  $\lambda/10$  optical quality. Holders for the wave plates and fiber couplers are made of Invar.

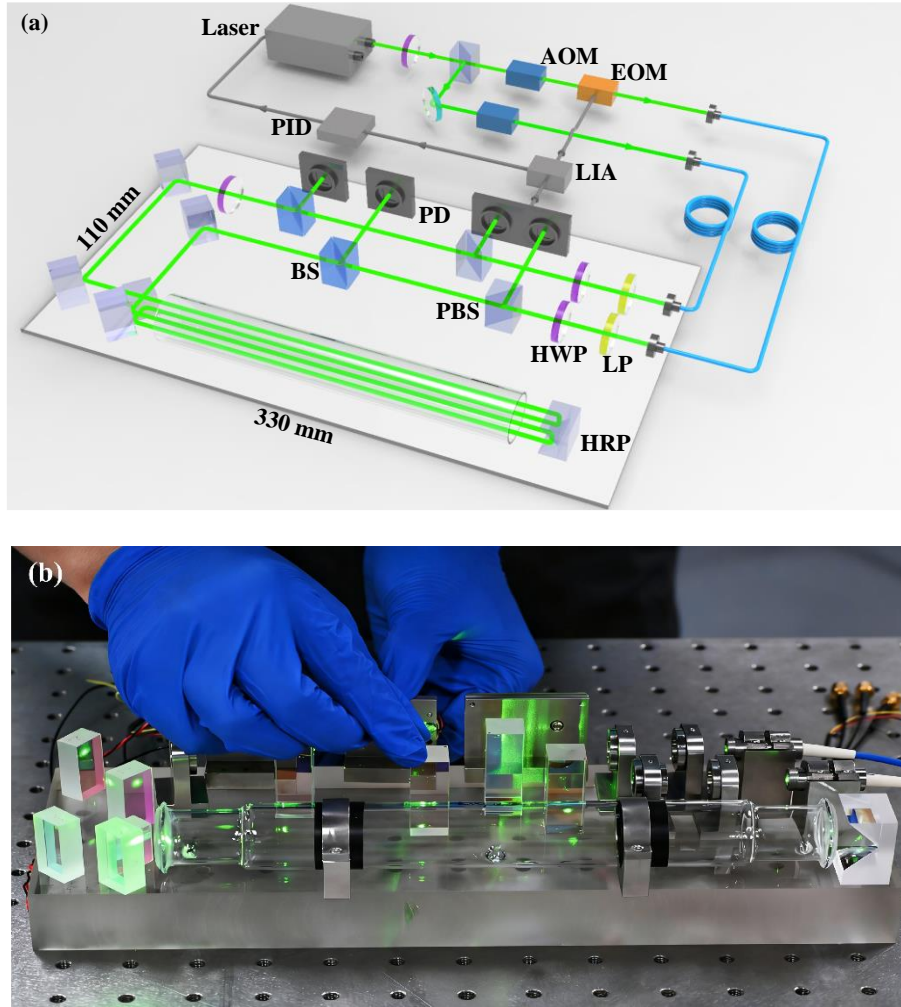


**Figure 1.** (a) Experimental system schematic diagram. HWP: half-wave plate; PBS: polarizing beam splitter; LP: linear polarizer; BS: beam splitter; PD: photo detector; BPD: balanced photodetector; LIA: lock-in amplifier; AOM: acousto-optic modulator; EOM: electro-optic modulator; HRP: hollow roof prism. (b) Photograph of the inside of the iodine spectroscopy module (ISM).

Inside the ISM, the pump and probe beams are coupled in via two fibres. The probe beam first passes through a half-wave plate and a PBS. A portion of the probe beam is reflected by the PBS to serve as a reference for the balanced photodetector (BPD). Another portion is diverted by a BS for optical power stabilization before being reflected by two mirrors into the iodine cell. Separately, part of the pump beam is likewise sampled by a BS for power stabilization. A half-wave plate is used to ensure that the pump and probe beams maintain orthogonal polarization. Inside the iodine cell, the incident powers are 5.3 mW (pump) and 0.8 mW (probe), with a beam radius of 2.2 mm for both beams. Within the cell, the two beams are spatially overlapped and propagate in opposite directions to cancel Doppler broadening caused by molecular thermal motion. Upon exiting the cell, the probe beam is reflected by a PBS to the BPD, where the corresponding photocurrent is subtracted from that of the reference light to obtain the MTS signal. All photodetectors are mounted on Invar holders and then epoxy-bonded onto the ULE substrate.

The iodine cell is an unsaturated cell<sup>25</sup> with a specified gas pressure. It is made of fused silica and incorporates wedged optical windows with a  $1^\circ$  angle to suppress parasitic back-reflections and etalon effects<sup>28,29</sup>. Both the inner and outer surfaces of the windows are antireflection-coated for 532 nm wavelength. The cell was fabricated by welding the glass components together. The inner volume was evacuated to a vacuum level of  $\sim 1 \times 10^{-7}$  Pa, and filled with triple-distilled

molecular iodine ( $^{127}\text{I}_2$ ) to a final pressure of 3.3 Pa. This pressure is chosen based on our past experience on regular saturated cells<sup>24</sup>. With a physical length of 250 mm and a clear aperture of 22 mm, the optical path length is extended to 1000 mm by using a four-pass configuration, achieved via a hollow roof prism positioned at the far end of the cell.

The error signal from the BPD is demodulated by a lock-in amplifier using quadrature detection to extract the in-phase component. This signal is processed by a servo system based on a PID algorithm for laser frequency stabilization. It is fed back to the laser PZT controller with a servo bandwidth of approximately 13 kHz, and simultaneously to the laser temperature controller with a bandwidth of a few hertz. The iodine-stabilized frequency system implements an automatic locking routine to maintain long-term operation. For automated program recognition, the laser frequency is locked to the R(56)32-0:a<sub>1</sub> transition line.

The stability of the iodine-stabilized system is characterized by beating the laser's 1064 nm output against an optical frequency comb (OFC)<sup>30,31</sup>, while the comb is locked to an optical frequency reference—specifically, a 30 cm ultra-stable cavity laser serving as the clock laser of an Al<sup>+</sup> optical frequency standard<sup>32,33</sup>. This cavity laser exhibits short-term fractional frequency stability of  $1.3 \times 10^{-16}$  at 1 s,  $2.2 \times 10^{-16}$  at 10 s, and  $5 \times 10^{-16}$  at 100 s<sup>34</sup>. Due to the frequency drift of the 30 cm cavity, a de-drift process was applied to the raw data.

During the stability measurement campaign all the electronics devices are referenced to a hydrogen-maser-based time-scale system, which is linked to UTC(National Institute of Metrology, China) via Global Navigation Satellite System (GNSS). The frequency uncertainty of this time-scale system<sup>33</sup>, as evaluated during absolute frequency measurements of the Al<sup>+</sup> optical clock, is  $1.4 \times 10^{-14}$ .

The beat signal between the 1064 nm laser output and OFC, which lies in the tens of megahertz range, is filtered, amplified and then downconverted to 1.5 MHz by mixing with a signal generator, followed by amplification, filtering, and input to a frequency counter (Keysight 53230A) for stability analysis.

Owing to the module's mechanical rigidity and active laser power stabilization, the spectroscopy linewidth approaches the theoretical Doppler-broadened limit at this pressure and at this laser power, which is about 580 kHz. The short-term fractional frequency instability, measured by the Allan deviation, reach  $5 \times 10^{-15}$  at 1 s averaging time (Fig. 2). This represents one of the best short-term performances reported for a vapor-cell standard and is currently limited by photodetector shot noise and residual laser frequency noise. The central achievement of this work is the medium-term stability (100–2,000 s). As shown in Fig. 2, the instability reaches a minimum of  $6.6 \times 10^{-16}$  at 1,000 s and remains at the  $10^{-16}$  level throughout the 100-2000 s window. This is the first demonstration of a vapor-cell optical frequency standard attaining  $10^{-16}$ -level instability in the medium-term regime.

When the averaging time is larger than 2,000 s, the frequency stability is slightly worse. This drift is attributed to residual effects within the temperature control and laser power control loop. Nevertheless, the instability remains below  $3 \times 10^{-15}$  for the averaging time of  $10^4$  s, demonstrating excellent medium-term holdover capability.

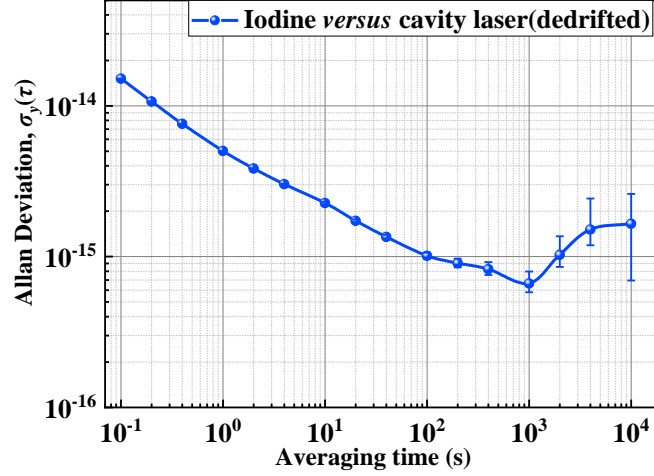


**Figure 2.** Frequency stability of the 532 nm iodine-stabilized laser.

To understand the frequency drift and the long-term stability, the systematic frequency shifts of the iodine-stabilized laser were investigated.

The temperature-induced frequency shift in the absorption cell originates from collisions between sample molecules or between molecules and the inner wall of the cell, which alter the quantum states of the molecules. This results in shifts of hyperfine energy levels and broadening of spectral lines. The impact of this noise source on the system frequency can be assessed by varying the temperature of the ISM. In this setup, the iodine cell is bonded inside the ISM, and the entire module is housed within a metal enclosure. The exterior of the housing is wrapped with thermal insulation to provide passive temperature control, ensuring that temperature fluctuations inside the ISM remain below 10 mK. By monitoring the frequency change as the temperature within the ISM is increased, the temperature-induced frequency shift coefficient was measured to be 146.5(2) Hz/K, as shown in Fig. 3(a), corresponding to a frequency uncertainty of 1.47 Hz.

Residual amplitude modulation (RAM) noise originates primarily from non-ideal effects such as polarization-related influences and birefringence in the electro-optic phase modulator, as well as parasitic interference within the optical path. Although the wedged EOM employed in our setup helps suppress this noise to some extent, it remains slightly sensitive to temperature variations. By subjecting the EOM to periodic temperature changes, we measured the temperature-dependent frequency shift induced by RAM to be  $-65.2(8)$  Hz/K, as shown in Fig. 3(b), corresponding to a frequency uncertainty of 0.65 Hz.

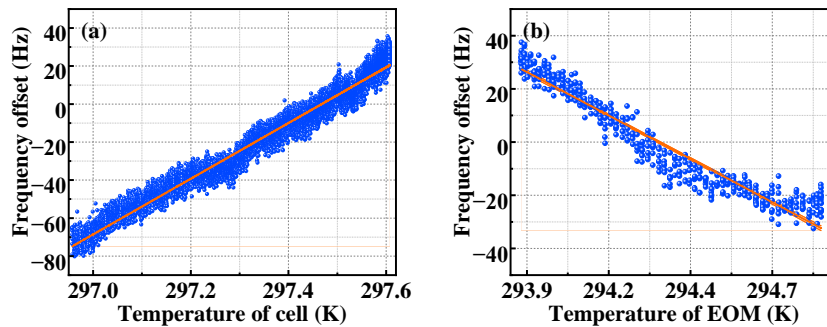


**Figure 3.** Relationship between the measured frequency offset and (a) temperature of the cell, (b) temperature of EOM. Orange lines indicate the linear fit to the data points.

In an alternating electromagnetic field, the rapid electric field oscillation between positive and negative amplitudes suppresses the first-order Stark effect in systems lacking a permanent electric dipole moment. However, this oscillation

concurrently enhances the second-order Stark effect, ultimately resulting in shifts of the energy levels. The R(56)32-0 transition line of iodine molecules corresponds to a magnetically insensitive state. The influence of the optical field on this transition is primarily manifested through the AC Stark effect induced by the optical electric field, which gives rise to spectral line frequency shifts, also referred to as power-induced frequency shifts.

By adjusting the optical power of the pump and probe beams before they enter the iodine cell, the power-induced frequency shift coefficients were measured to be 330(6) Hz/mW for the pump beam and 1138(6) Hz/mW for the probe beam, as shown in Fig. 4. In the experiment, the pump beam power entering the cell was 5.3 mW. After power stabilization, the power uncertainty remained below 7  $\mu$ W, resulting in a corresponding frequency uncertainty of 2.31 Hz. The probe beam power entering the cell was 0.8 mW and the power uncertainty is 0.6  $\mu$ W, corresponding to a frequency uncertainty of 0.68 Hz.

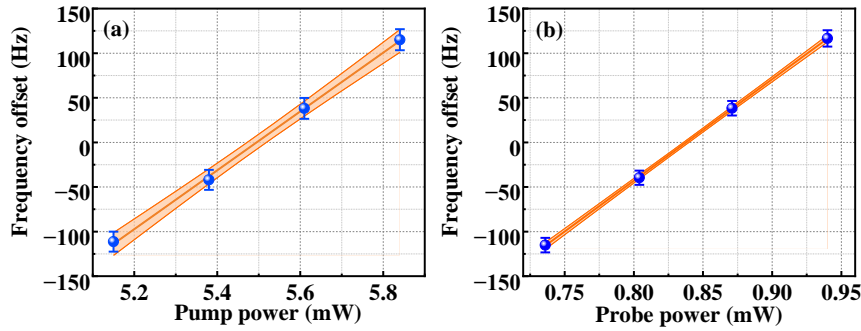


**Figure 4.** Relationship between the measured frequency offset and (a) pump power, (b) probe power. Orange lines indicate the linear fit to the data points.

In laser frequency stabilization based on the modulation transfer spectroscopy, the modulation parameter, including the modulation frequency, modulation depth and the demodulation phase will all influence the locked laser frequency. By varying the modulation frequency of the EOM, the induced frequency shift was measured to be 61(1) Hz/kHz, as shown in Fig. 5(a), resulting in an uncertainty of 0.06 Hz. Since the frequency discrimination signal is obtained by comparing the different absorption intensities of the left and right sidebands of phase-modulated light in a nonlinear absorption medium, the selection of modulation depth is crucial. By varying the modulation voltage, the frequency shift due to modulation depth was measured to be  $-306(15)$  Hz, as shown in Fig. 5(b), with an uncertainty of 0.31 Hz. The demodulation phase shift coefficient was determined to be  $-8.6(2)$  Hz/degree by adjusting the phase of the demodulation signal, as illustrated in Fig. 5(c). Since the lock-in amplifier employs quadrature demodulation, its associated frequency shift is considered negligible. The phase jitter of the lock-in amplifier remains well below 0.001 degree, corresponding to an uncertainty of 0.01 Hz.

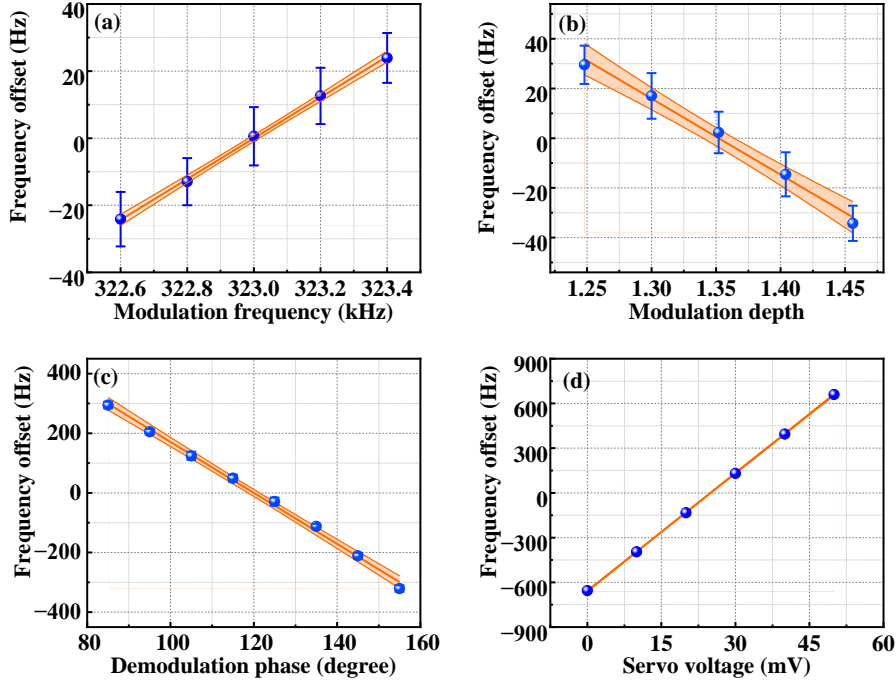


**Figure 5.** Relationship between the measured frequency offset and (a) modulation frequency, (b) modulation depth, (c) demodulation phase, and (d) servo voltage. Orange lines indicate the linear fit to the data points.

In the experiments, the frequency at the zero-crossing point of the error signal is typically selected as the frequency discrimination point. The frequency discrimination slope of this servo system is measured to be 26.40(4) Hz/mV, as shown in Fig. 5(d). Given that voltage offset fluctuations consistently remain below 10  $\mu$ V, the corresponding frequency uncertainty attributable to electronic servo noise amounts to approximately 0.26 Hz.

The most significant contributions to the estimated frequency uncertainty of the compact iodine-stabilized laser are summarized in Table 1. As can be seen from Table 1, the primary sources of noise are the iodine cell temperature, EOM temperature, and optical power fluctuations. The total uncertainty was estimated to be 2.92 Hz (relatively  $5.2 \times 10^{-15}$ ), in line with the long-term stability of the frequency.

**Table 1.** Most significant contributions to the uncertainty of the iodine-stabilized laser

Source	Sensitivity	Uncertainty (Hz)
Temperature of cell	146.5(2) Hz/K	1.47
Temperature of EOM	-65.2(8) Hz/K	0.65
Pump power	330(6) Hz/mW	2.31
Probe power	1138(6) Hz/mW	0.68
Modulation frequency	61(1) Hz/kHz	0.06
Modulation depth	306(15) Hz	0.31
Demodulation phase	-8.6(2) Hz/degree	0.01
Servo electronics	26.40(4) Hz/mV	0.26
<b>Total</b>		<b>2.92</b>
<b>Relative uncertainty</b>		<b><math>5.2 \times 10^{-15}</math></b>

## Discussion and Conclusions

Our work decisively overturns the prevailing notion that vapor-cell optical frequency standards are intrinsically limited to

fractional frequency instabilities in the  $10^{-14}$  to  $10^{-15}$  range. By demonstrating medium-term (minute to hour) stability at the  $10^{-16}$  level with an iodine-stabilized laser—a first for any vapor-cell optical standard—we redefine the performance ceiling for compact atomic clocks. This achievement was realized not by mitigating a single fundamental limit, but through a holistic stability-engineering approach. We designed a system around a passively stable, drift-immune monolithic spectroscopic core and implemented precision environmental control over critical active components, thereby suppressing technical noise to reveal a shot-noise-limited floor near 1000 s. This result proves that the classical barriers of homogeneous broadening and collisional shifts in room-temperature vapors are not ultimate boundaries; with disciplined system engineering, vapor-cell standards can access performance domains once exclusive to the most advanced cold-atom platforms.

The implications of this paradigm shift are both scientific and technological. Scientifically, it invites a re-evaluation of the potential of other vapor-cell systems, such as those based on rubidium or cesium. Our “monolithic-core + targeted-control” architecture provides a generalizable blueprint for pushing these platforms beyond their presumed stability limits. Technologically, it delivers a concrete path to packaging cold-atom-optical-clock-grade performance into a robust, compact format suitable for field deployment. The inherent insensitivity of the monolithic core to environmental perturbations, combined with modular noise suppression, directly addresses key challenges like vibration-induced phase noise and thermal drift, which have historically hindered the transition of precision photonics from the lab to real-world applications.

Looking forward, the clear next frontier is the management of long-term frequency drift, a characteristic common to all sealed vapor-cell standards. Unravelling its physical origins—whether from slow gas-composition changes, wall interactions, or residual thermal transients on the optical or electrical components—will be crucial for achieving fully autonomous operation as a primary standard. Promising mitigation strategies include the development of novel thermal management and optimized voltage reference in the control circuits. Even at its current performance, our system’s stability and low drift already enable compelling applications, such as serving as a local oscillator in satellite navigation ground stations or distributed sensor networks for several days without calibration.

The attainment of  $10^{-16}$  medium-term stability unlocks a new application space for compact optical standards. These devices can now function as ultra-stable flywheel oscillators to maintain phase coherence across geographically separated sites, such as in next-generation GNSS or very-long-baseline interferometry networks. Furthermore, they enable high-resolution geopotential measurements on mobile platforms and can serve as synchronized time sources for emerging distributed quantum sensing networks. By breaking the  $10^{-15}$  barrier, we move beyond merely miniaturizing laboratory instruments and towards embedding fundamental metrological performance into the fabric of field-based science and technology. This work thus repositions vapor-cell optical standards as cornerstone technologies for future advancements in precision timing, navigation, and fundamental physics beyond the laboratory walls.

**Funding.** National Key Research and Development Program of China (2022YFB3904000, 2022YFC2204002) and Strategic Priority Research Program of the Chinese Academy of Sciences (XDA0520503).

**Acknowledgments.** The authors gratefully thank Jingbiao Chen and Duo Pan for their valuable advice.

**Data availability.** Raw data that support the findings of this study are available from the corresponding author upon reasonable request.

## References

1. McGrew, W. F. et al. Atomic clock performance enabling geodesy below the centimetre level. *Nature* **564**, 87-90 (2018).
2. Oelker, E. et al. Demonstration of  $4.8 \times 10^{-17}$  stability at 1 s for two independent optical clocks. *Nature Photon.* **13**, 714 (2019).
3. Ushijima, I., Takamoto, M., Das, M., Ohkubo, T., and Katori, H. Cryogenic optical lattice clocks. *Nature Photon.* **9**, 185 (2015).
4. Hilton, A. P. et al. Demonstration of a mobile optical clock ensemble at sea. *Nature Commun.* **16**, 6063 (2025).

5. Marshall, M. C. et al. High-Stability Single-Ion Clock with  $5.5 \times 10^{-19}$  Systematic Uncertainty. *Phys. Rev. Lett.* **135**, 033201 (2025).
6. Schuldt, T. et al. Optical clock technologies for global navigation satellite systems. *GPS Solut.* **25**, 83 (2021).
7. Wegehaupt, T. et al. Towards Compact, Robust and Highly Stable Optical Frequency References for Space Applications. *J. Phys. Conf. Ser.* **2889**, 012012 (2024).
8. Döringshoff, K. et al. A flight-like absolute optical frequency reference based on iodine for laser systems at 1064 nm. *Appl. Phys. B* **123**, 1–8 (2017).
9. Asaki, Y., Pampliega, B. A., Edwards, P. G., Iguchi, S. and Murphy, E. J., *Nat. Rev. Methods Primers* **3**, 89 (2023).
10. Eickhoff, M. L. and Hall, J. L. Optical frequency standard at 532 nm. *IEEE Trans. Instrum. Meas.* **44**, 155–158 (1995).
11. Ye, J., Ma, L. S., and John, L. H., Molecular Iodine Clock. *Phys. Rev. Lett.* **87**, 270801 (2001).
12. Riehle, F., Gill, P., Arias, F. and Robertsson, L. The CIPM list of recommended frequency standard values: guidelines and procedures *Metrologia* **55**(2), 188 (2018).
13. Hong, F.-L. et al. Frequency reproducibility of an iodine-stabilized Nd:YAG laser at 532 nm. *Opt. Commun.* **235**, 377 (2004).
14. Zang, E. J., et al. Realization of Four-Pass I<sub>2</sub> Absorption Cell in 532-nm Optical Frequency Standard. *IEEE Trans. Instrum. Meas.* **56**, 673 (2007).
15. Lazar, J., Hrabina, J., Jedlicka, P., and Cip, O. Absolute frequency shifts of iodine cells for laser stabilization. *Metrologia* **46**, 450 (2009).
16. Nyholm, K., Merimaa, M., Ahola, T. and Lassila, A. Frequency Stabilization of a Diode-Pumped Nd:Yag Laser at 532 nm to Iodine by Using Third-Harmonic Technique *IEEE Trans. Instrum. Meas.* **52**(2) 284-287 (2003).
17. Cheng, F. H. et al. A 532 nm molecular iodine optical frequency standard based on modulation transfer spectroscopy, *Chin. Phys. B* **30**, 050603 (2021).
18. Zhang, J. R. et al. Development of High-Reliability Solid-State Laser for Space Applications. *Chin. J. Lasers* **53**(02), 0201004 (2026).
19. Kuschewski, F. et al. COMPASSO mission and its iodine clock: outline of the clock design. *GPS Solutions* **28**, 10 (2024).
20. Döringshoff, K. et al. Iodine frequency reference on a sounding rocket. *Phys. Rev. Appl.* **11**, 054068 (2019).
21. Schuldt, T. et al. Development of a compact optical absolute frequency reference for space with  $10^{-15}$  instability. *Appl. Opt.* **56**, 1101 (2017).
22. Schuldt, T. et al. Absolute laser frequency stabilization for LISA, *Int. J. Mod. Phys. D* **28**, 1845002 (2019).
23. Roslund, J. D. et al. Optical clock at sea, *Nature* **628**(8009), 736-740 (2024).
24. Zhang, Z. Q. et al. An ultra-stable laser based on molecular iodine with a short-term instability of  $3.3 \times 10^{-15}$  for space based gravity missions. *Class. Quantum. Grav.* **40**, 225001 (2023).
25. Zhang, Z. Q. et al. High performance molecular iodine optical reference using an unsaturated vapor cell. *Rev. Sci. Instrum.* **95**, 063003 (2024).
26. Gamache, R. R. and Vispoel, B. On the temperature dependence of half-widths and line shifts for molecular transitions in the microwave and infrared regions. *J. Quant. Spectrosc. Radiat. Transfer.* **217**, 440-452 (2018).
27. Chen, S. Y. and Takeo, M. Rev. Broadening and Shift of Spectral Lines Due to the Pressure of Foreign Gases. *Mod. Phys.* **29**(1), 20-73 (1957).
28. Oulehla, J. et al. Influence of coating technology and thermal annealing on the optical performance of AR coatings in iodine-filled absorption cells. *Opt. Express* **27**(7), 9361-9371 (2019).
29. Hrabina, J. et al. Spectral properties of molecular iodine in absorption cells filled to specified saturation pressure. *Appl. Opt.* **53**, 7435-7441 (2014).
30. Cundiff, S. T. and Ye, J. Colloquium: Femtosecond optical frequency combs. *Rev. Mod. Phys.* **75**, 325 (2003).
31. Diddams, S. A., Vahala, K. and Udem, T. Optical frequency combs: Coherently uniting the electromagnetic spectrum. *Science* **369**, eaay3676 (2020).
32. Ma, Z. Y. et al. Quantum-logic-based  $^{25}\text{Mg}^{+}$ - $^{27}\text{Al}^{+}$  optical frequency standard for the redefinition of the SI second. *Phys. Rev. Appl.* **21**, 044017 (2024).
33. Ma, Z. Y. et al. Absolute frequency measurement of an  $\text{Al}^{+}$  ion optical clock through a GNSS link to the SI second. *Metrologia*, **62**, 045002 (2025).
34. Wang, Z. Y. et al. Noise characterization of an ultra-stable laser for optical clocks. *Rev. Sci. Instrum.* **95**, 053002 (2024).